Whitmarsh, R.B., Sawyer, D.S., Klaus, A., and Masson, D.G. (Eds.), 1996
Proceedings of the Ocean Drilling Program, Scientific Results, Vol. 149

11. EVOLUTION OF THE IBERIAN PASSIVE MARGIN AS REFLECTED IN SAND PROVENANCE[1]

Kathleen M. Marsaglia,[2] Juan Carlos García y Barragán,[2] Ivan Padilla,[2] and Kitty L. Milliken[3]

ABSTRACT

On Ocean Drilling Program Leg 149, a transect of drill sites across the ocean/continent transition along the western margin of Iberia recovered Mesozoic synrift to Cenozoic postrift sedimentary sequences above a series of basement highs. Sand detrital modes were determined for samples taken from Jurassic to Pleistocene sandy turbidite layers from these sites. The terrigenous sand recovered on ODP Leg 149 is predominantly quartzofeldspathic with a lesser metamorphic and sedimentary lithic component. There appears to be a distinct link between grain size and composition within the Cenozoic samples, probably resulting from a combination of transport and depositional history. Fine sand detrital modes reflect the overall passive margin, rift-to-drift evolution and show a crude basement unroofing trend from the Mesozoic to the Cenozoic. The detrital modes of Cenozoic very fine sand are a function, to some degree, of a superposed regional compressional tectonic event that resulted in a minor increase in metamorphic lithic content during the Oligocene and Miocene, perhaps associated with enhanced uplift on the adjacent Iberian Peninsula. Overall, results from this study provide a preliminary model for passive margin sand provenance.

INTRODUCTION

During Ocean Drilling Program (ODP) Leg 149, a transect of sites (897-901) was drilled across the ocean/continent transition along the western margin of Iberia, a predominantly nonvolcanic passive margin (Fig. 1; Sawyer, Whitmarsh, Klaus, et al., 1994). At these sites, Mesozoic synrift to Cenozoic postrift sedimentary sequences were recovered above a series of basement highs (Fig. 2).

The thickest (~ 700 m) and most stratigraphically complete sedimentary sequences were recovered at Sites 897 and 900 (Fig. 3; Sawyer, Whitmarsh, Klaus, et al., 1994). The pre-Eocene to Cretaceous sedimentary units are lithologically diverse and include mass-flow deposits at Sites 899 and 897 and Cretaceous serpentinite breccias at Site 899. Oligocene to middle Miocene units at Sites 897-900 consist of interbedded to interlaminated contourites, turbidites, hemipelagites, and pelagites, which are overlain, in turn, by Miocene to Pleistocene turbidite, hemipelagite, and pelagite successions (Fig. 3). The change from predominantly contourite to turbidite sedimentation occurs in the middle Miocene (Fig. 4), concurrent with a compressional phase of regional deformation (Sawyer, Whitmarsh, Klaus, et al., 1994).

In general, the Leg 149 sediments are composed dominantly of terrigenous mud, with a significant calcareous pelagic component, and lesser amounts of sand (Fig. 3). Thin sand laminae occur throughout the Jurassic to Pleistocene successions cored at all five sites, but are most prevalent within the Pliocene and Cretaceous sections at Site 897, within the Pleistocene and Pliocene sections at Site 898, and within the Paleogene and Miocene sections at Site 900. Terrigenous sand, as opposed to bioclastic sand, is most common in the Pleistocene to Pliocene sections at Sites 897 and 898. The composition and provenance of the Jurassic to Pleistocene terrigenous sand is the focus of this paper.

[1]Whitmarsh, R.B., Sawyer, D.S., Klaus, A., and Masson, D.G. (Eds.), 1996. *Proc. ODP, Sci. Results,* 149: College Station, TX (Ocean Drilling Program).
[2]Department of Geological Sciences, University of Texas at El Paso, El Paso, TX 79968, U.S.A.
[3]Department of Geological Sciences, University of Texas at Austin, Austin, TX 78712, U.S.A.

METHODS

A total of 144 samples was collected during Leg 149 for use in this study. Sample intervals for Sites 897, 898, 899, 900, and 901 are shown in Figure 3. Unconsolidated samples were air-dried and then hand-sieved for the sand fraction; for each very fine to fine sand sample the sand concentrate was sprinkled onto a glass slide spread with epoxy; the epoxy was cured, and then the sand/epoxy mixture was ground to a thickness of 30 microns. For coarser samples, for which grain orientation might be a problem using this method, a second stage was added: the sand/epoxy mixture was ground flat, and then another slide was attached with epoxy to the smoothed surface and the original slide was ground away. Lithified samples were vacuum-impregnated with blue-dyed epoxy under high pressure prior to thin-section preparation. Thin sections were stained for potassium and calcium feldspar recognition using the method outlined in Marsaglia and Tazaki (1992).

Approximately two-thirds of the shipboard samples collected for this investigation proved unsuitable for sand provenance studies in that they contained an insufficient sand fraction. Many of the unsuitable samples are coarse silts/siltstones and bioclastic sediments/rocks. Only 50 samples contained sufficient siliciclastic sand for point-counting purposes (Appendix). For these samples, 250 to 300 points were counted per thin section using the Gazzi-Dickinson method of point counting (Dickinson, 1970; Ingersoll et al., 1984). The grid spacings used were larger than the maximum grain size, and thus fewer points were counted for some coarser samples and for samples with only a minor terrigenous component. Uniformity among operators was maximized by recounting the thin sections by multiple operators and by frequent cross-verification of grain types throughout the counting process.

Counted grains were placed into 22 monomineralic and polymineralic compositional categories (Table 1). Because the sand-sized bioclastic component in some samples was so great, bioclastic debris was not tallied in six samples ("nc" in the Bio category in the Appendix). Point-count categories and recalculated parameters (e.g., QFL, QmKP, LmLvLs) are defined in Table 1, raw point-count data are presented in the Appendix, and recalculated parameters are listed in Table 2. Recalculated parameters, means, and standard deviations were calculated using a Quattro Pro spreadsheet program. For each sample, mean grain (sand) size was petrographically estimated; these data are listed in Table 2.

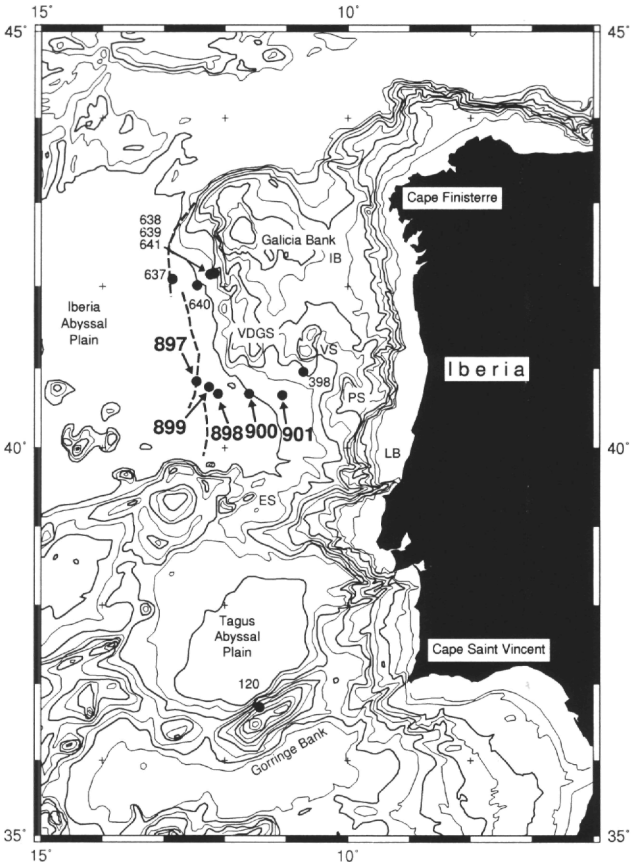

Figure 1. Location map for Sites 897 through 901 drilled on Leg 149, modified from Whitmarsh et al. (1994). Bathymetry is in meters, with bold contours at 1000-m intervals. The other numbered sites were drilled on Legs 13, 47B, and 103. The dashed lines near Sites 637 and 897 mark the predicted positions of peridotite ridges. Location abbreviations are as follows: ES = Estremadura Spur; LB = Lusitanian Basin; PS = Porto Seamount; VS = Vigo Seamount; VDGS = Vasco da Gama Seamount; IB = Galicia Interior Basin.

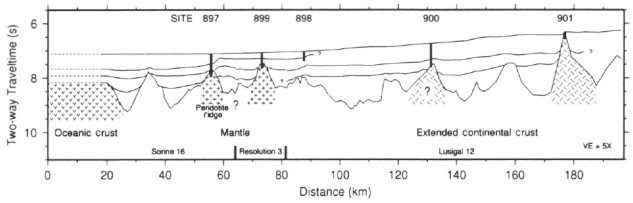

Figure 2. Schematic cross section across the Iberia Margin with Leg 149 site locations, sediment distribution, and inferred basement lithology and configuration, modified from Whitmarsh et al. (1994). This composite section was constructed using a series of seismic lines along a transect of the Leg 149 sites. Symbols reflect the variable basement lithology across the margin. The westernmost part of the section is underlain by oceanic crust. Drilling results indicate that Sites 897 and 899 are underlain by serpentinized peridotite (upper mantle), whereas Site 900 is underlain by sheared gabbro with mid-oceanic-ridge-basalt affinities. The Jurassic pre- or synrift sedimentary rocks recovered at Site 901 most likely overlie extended continental crust.

RESULTS

Sand Description

In general, sand recovered at the Leg 149 sites is composed dominantly of quartz, feldspar, and metamorphic lithic fragments, with locally abundant mica (Appendix; Pls. 1, 2). The quartz grains exhibit slightly undulose to straight extinction and occur as individual monocrystalline grains and sand-sized components of lithic fragments (Pls. 1, 2). Polycrystalline quartz grains, including chert, make up less than 5% of the framework grains (Appendix; Pl. 1). Both potassium and plagioclase feldspar are present in moderate to minor amounts, and most occur as individual monocrystalline grains, rather than within feldspathic (plutonic and high-grade metamorphic) lithic fragments (Pls. 1, 2). Feldspar grains range from fresh to altered, with alteration products including sericite and kaolinite (Pls. 1, 2). Unstained albitic feldspar is rare, and generally very altered (Pl. 2, Fig. 2). Muscovite and biotite also make up a significant proportion of the framework grains (Table 2; Pl. 1, Fig. 6), with lesser amounts of chlorite. Biotite flakes exhibit brown to green pleochroism and are commonly altered to opaque minerals, clay minerals, and chlorite.

The lithic component is dominantly fragments of low-grade metamorphic and metasedimentary rocks. The metamorphic lithic fragments are mostly quartz-mica tectonite and polycrystalline mica, with lesser amounts of quartz-feldspar-mica aggregate (Pls. 1, 2). Sedimentary lithic fragments, such as shale/argillite, sedimentary or dirty chert, and micritic/microsparite carbonate, are significant components in some samples (Pls. 1, 2). In contrast, fragments of variably altered microlitic, vitric, and felsitic volcaniclastic debris are generally rare (Pl. 2).

Bioclastic material is present in each sample. A wide variety of calcareous (e.g., foraminifers, shell fragments) and siliceous (predominantly sponge spicules) bioclasts are present in varying amounts. Because of their dominance in a few samples ("nc" in the Bio column of the Appendix), they were not tallied into the total points counted.

A few samples have a significant percentage of opaque grains, but surprisingly few nonopaque dense minerals are present (Appendix). The most common nonopaque dense minerals are green hornblende, zircon, and garnet (Pl. 1), with lesser amounts of augite, zoisite, epidote, and sphene. Rare, isolated grains of tremolite, tourmaline, enstatite, and rutile are also present. The heavy mineral fraction is generally finer grained than the associated siliciclastic components. Other minor components include glauconite (Pl. 1), plant fragments, carbonate (authigenic?), and serpentine.

Sand Detrital Modes

The range of sand compositions within Leg 149 cores is shown in Figures 5 and 6. In general, most samples are quartzofeldspathic with only a minor lithic component. Sand from Sites 899 and 901 is more enriched in lithic fragments, and a few samples from Sites 897 and 898 are very feldspathic (Fig. 5). In terms of monomineralic components, quartz and potassium feldspar are the most common, but a number of samples from Sites 897 and 898 are significantly enriched in plagioclase feldspar (Fig. 6). Although lithic proportions (LmLv-Ls) were calculated (see Tables 1, 2), these are not presented in ternary format because of the dominance of metamorphic lithic fragments in most samples.

Relationship of Composition to Grain Size

The Gazzi-Dickinson method of point counting was used in this study to minimize grain-size effects on sand composition (Dickinson, 1970; Ingersoll et al., 1984). When sand samples are grouped by grain size, however, there appears to be a direct relationship between grain size and the QFL and QmKP detrital modes. The Cenozoic medium sand samples are much more quartzose than the fine to very fine sand samples, and there is a progressive trend in mean QFL and QmKP compositions toward more feldspathic compositions with decreasing grain size (Fig. 7). The distinction between medium, fine, and very fine sand compositions is even more pronounced for the

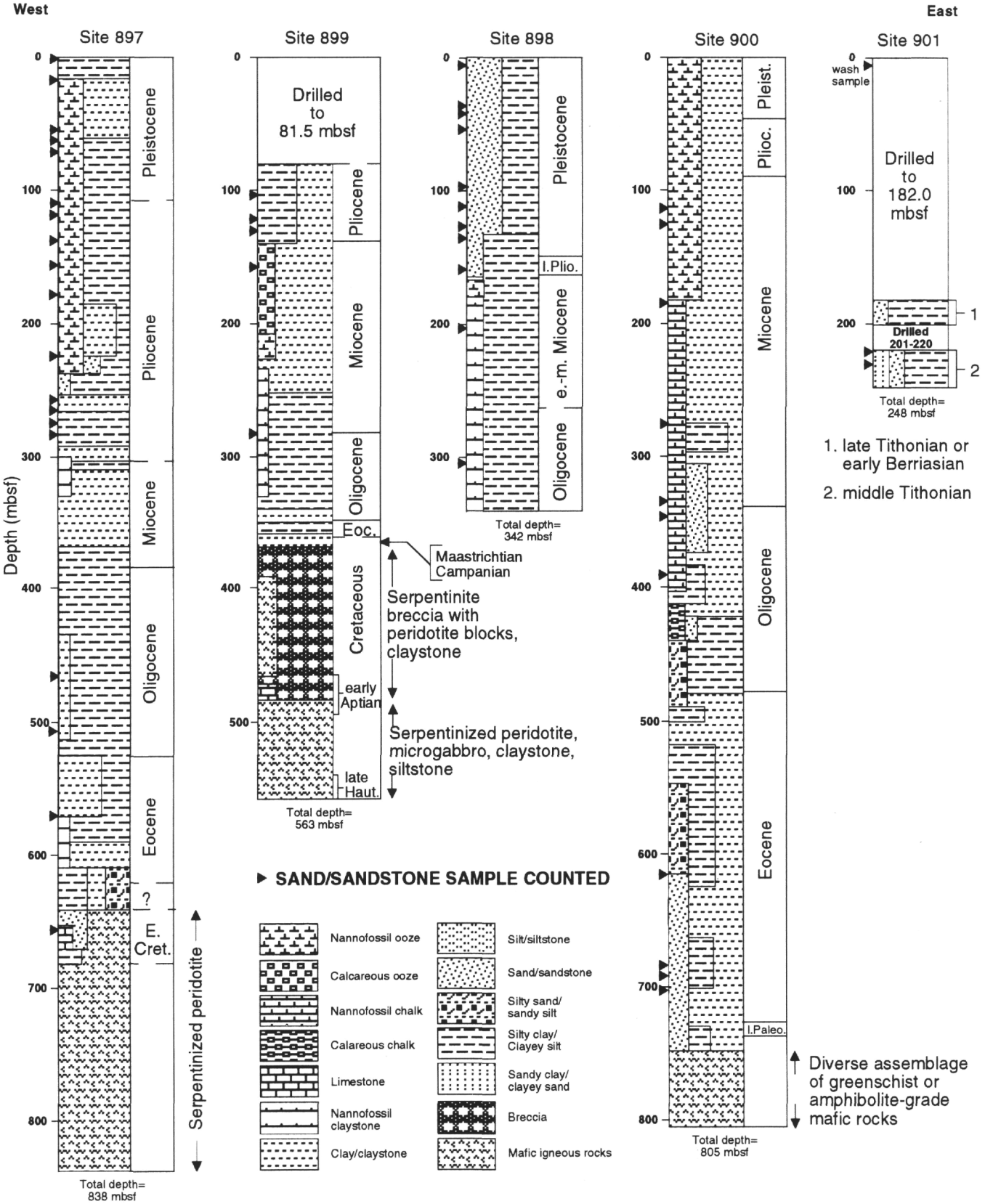

Figure 3. Simplified lithologic columns for Leg 149 sites modified from Whitmarsh et al. (1994). Sample intervals are indicated for the sand/sandstone samples point counted in this study (Appendix, Table 2).

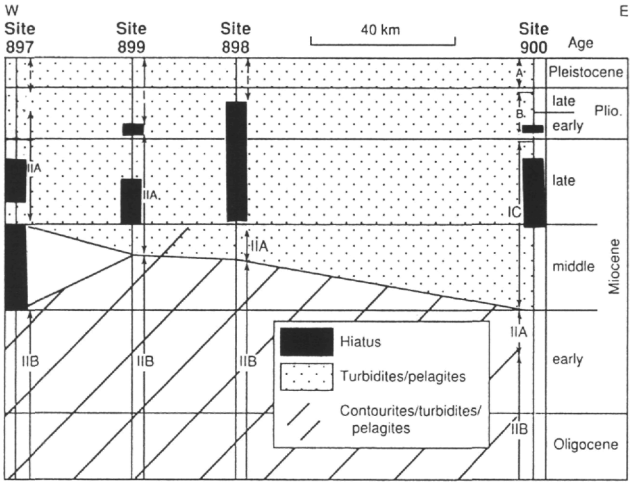

Figure 4. Stratigraphic correlation chart for the Leg 149 sites. Depositional hiatuses are defined by biostratigraphic data (see Sawyer, Whitmarsh, Klaus, et al. [1994] for further information). Contourites were differentiated from turbidites, in part, by composition (contourites have abundant siliceous allochems and reworked carbonate) and by evidence of reworking by contour currents. Lithostratigraphic units are labeled at each site.

Pleistocene samples, which exhibit a similar trend toward more feldspathic compositions with decreasing grain size (Fig. 8). Also, Pleistocene very fine sand is slightly enriched in plagioclase feldspar and lithic fragments with respect to the fine to medium sand (Fig. 8).

In their analysis of the traditional vs. the Gazzi-Dickinson petrographic point-counting methods, Ingersoll et al. (1984) counted unsieved sand samples and, for comparison, various sieved fractions from these same samples. A similar analysis of Leg 149 samples would be useful in deciphering the nature of the relationship between feldspar content and grain size as outlined in Figures 7 and 8; however, further subdivision (sieving) of these samples is generally precluded by the small sample volume (~5 cm^3) and high matrix to sand ratio.

Relationship of Composition to Sediment Age

Because of the grain-size correlations outlined above, sand samples were first grouped by grain size prior to further subdivision by age. The large number of very fine sand samples provides the best statistical sample (four Pleistocene, 10 Pliocene, six Miocene, five Oligocene, and four Eocene) for determining age relationships. The means and fields of variation for these age subsets exhibit a large amount of overlap (Fig. 9), but the Oligocene and Miocene samples show a higher range in QFL lithic proportions, as compared with the Eocene, Pliocene, and Pleistocene samples. In terms of monomineralic proportions, the Eocene and Oligocene samples are significantly enriched in potassium feldspar with respect to younger samples, and there appears to be a shift toward more plagioclase-rich sand from the Miocene to the Pleistocene (Fig. 10).

The limited number of fine sand samples allows for only a general comparison of detrital modes, but across a greater time span (Mesozoic to Cenozoic). A crude QFL compositional trend can be outlined, with lithic-rich Jurassic sand (stone) and lithic-poor Pleistocene sand as end-members (Fig. 11). In terms of QmKP proportions, again, some crude temporal trends are apparent (Fig. 11): the Mesozoic samples are the most quartzose with lesser plagioclase, the Eocene to Oligocene samples have the highest K-feldspar content, and the youngest Miocene to Pleistocene sediments exhibit compositions between these two end-members.

Table 1. Counted and recalculated parameters.

Counted parameters:	
Qp:	Polycrystalline quartz
Qm:	Monocrystalline quartz
P:	Plagioclase feldspar
K:	Potassium feldspar
Fu:	Unstained (Na ?) feldspar
Lv:	Volcanic lithic
Lmm:	Polycrystalline mica lithic
Lmt:	Quartz-mica tectonite lithic
Lma:	Quartz-feldspar-mica aggregate lithic
Lsa:	Argillite-shale lithic
Lsch:	Sedimentary chert or cherty argillite lithic
Lsc:	Sedimentary carbonate lithic
Mu:	Muscovite
Biot:	Biotite
Op:	Opaque dense minerals
D:	Nonopaque dense minerals
Bio:	Siliceous and calcareous microfossils and bioclasts
Glau:	Glauconite
Other:	Other miscellaneous and unidentified grains
Pl:	Plant (organic) matter
Carb:	Carbonate minerals
Serp:	Detrital serpentine
Total points:	Total points counted
Q = Qm + Qp	F = P + K + Fu
L = Lm + Lv + Ls	Lm = Lmm + Lmt + Lma
	Ls = Lsa + Lsc + Lsch

Recalculated parameters:	
QFL%Q = 100 × Q/(Q + F + L)	LmLvLs%Lm = 100 × Lm/L
QFL%F = 100 × F/(Q + F + L)	LmLvLs%Lv = 100 × Lv/L
QFL%L = 100 × L/(Q + F + L)	LmLvLs%Ls = 100 × Ls/L
QmKP%Qm = 100 × Qm/(Qm + F)	
QmKP%P = 100 × (P + Fu)/(Qm + F)	
QmKP%K = 100 × K/(Qm + F)	
P/F = (P + Fu)/F	
Fr%M = (Mu + Biot)/(Total points)	

DISCUSSION

Composition and Grain-Size Variations

The compositional variations associated with grain size in the Leg 149 sand samples (Figs. 7, 8) could be attributed to a number of factors. First, this relationship could be a function of different provenance for finer vs. coarser grained turbidites: the turbidites fed from more proximal canyons may be coarser, whereas more distant canyons would supply finer turbidites to the same site, because of the longer transport distance. Second, the source region for the coarser and finer turbidites may be the same geographic region of the shelf, with grain-size variations a function of sediment derivation from different shelf depositional systems; for example, the medium, well-rounded quartzose sand might be derived from beach to shelf environments, whereas the finer, more angular, feldspathic sand may better tie to fluvial-deltaic environments. Compositional and textural differences among samples would therefore be linked to transport history. Third, given a uniform source of both coarse and fine turbidites, an inherent difference in size fractions could be associated with source-rock textural variations (e.g., relative crystal sizes of feldspar and quartz in source rocks) or with relative abrasion rates during transport (e.g., preferential breakdown of feldspar into a finer fraction because of the presence of cleavage). A combination of transport history and depositional environment controls on sand composition seems most plausible for the Iberia Margin turbidites. Results from a study of Pennsylvanian sandstones in Colorado by Kairo et al. (1993) support this interpretation, in that they link higher sand maturity in the foreshore area, as compared with offshore and alluvial regions, to the abrasion and mechanical breakdown of feldspar. Furthermore, studies of modern sand indicate that the framework mineralogy of beach sand is more mature than associated fluvial sand (Sedimentation Seminar, 1988).

Table 2. Recalculated parameters.

Core, section, interval (cm)	Depth (mbsf)	Age	Grain size	QFL (%Q)	QFL (%F)	QFL (%L)	QmKP (%Qm)	QmKP (%P)	QmKP (%K)	LmLvLs (%Lm)	LmLvLs (%Lv)	LmLvLs (%Ls)	P/F	Fr%M
149-														
897C-7R-1, 86–88	109.06	P	1	49.1	41.8	9.1	54.0	38.0	8.0	80.0	0.0	20.0	0.83	21.7
897C-2R-1, 142–144	61.32	P	1	17.1	75.2	7.8	18.5	67.2	14.3	90.0	0.0	10.0	0.82	32.7
897A-6R-5, 11–13	51.71	P	1	60.8	21.1	18.1	74.3	6.6	19.2	100.0	0.0	0.0	0.26	15.0
898A-5H-4, 49–51	42.72	P	1	36.9	56.6	6.6	39.5	26.5	34.1	92.3	0.0	7.7	0.44	18.3
			Avg	41.0	48.7	10.4	46.6	34.6	18.9	90.6	0.0	9.4	0.59	21.9
			Std	16.2	19.8	4.5	20.4	21.9	9.6	7.1	0.0	7.1	0.25	6.7
897C-8R-1, 92–94	118.82	Pl	1	28.1	56.3	15.6	33.3	57.0	9.6	100.0	0.0	0.0	0.86	32.7
897C-10R-2, 8–10	138.78	Pl	1	58.4	27.6	14.0	67.9	3.8	28.3	100.0	0.0	0.0	0.12	5.3
897C-24R-1, 78–80	273.08	Pl	1	63.3	21.8	14.8	74.4	3.1	22.6	100.0	0.0	0.0	0.12	10.3
897C-25R-CC, 0–2	283.98	Pl	1	58.6	37.9	3.4	60.7	9.7	29.6	100.0	0.0	0.0	0.25	21.3
897C-23R-2, 109–111	265.29	Pl	1	45.1	50.3	4.6	47.3	29.5	23.3	100.0	0.0	0.0	0.56	23.0
897C-14R-3, 104–106	179.84	Pl	1	60.1	36.4	3.5	62.3	11.6	26.1	100.0	0.0	0.0	0.31	30.3
897C-22R-3, 9–11	256.09	Pl	1	65.8	22.5	11.7	74.5	5.9	19.6	100.0	0.0	0.0	0.23	6.7
898A-18X-1, 142–145	159.52	lPl	1	13.6	77.3	9.1	15.0	48.3	36.7	83.0	0.0	17.0	0.57	35.7
899A-6R-1, 37–39	130.07	Pl	1	60.2	35.0	4.9	63.2	17.0	19.8	100.0	0.0	0.0	0.46	3.7
899A-5R-1, 33-35	120.43	Pl	1	66.4	14.0	19.6	82.6	2.3	15.1	100.0	0.0	0.0	0.13	7.7
			Avg	52.0	37.9	10.1	58.1	18.8	23.1	98.3	0.0	1.7	0.36	17.7
			Std	16.8	18.0	5.5	19.7	18.7	7.3	5.1	0.0	5.1	0.23	11.7
898A-22X-4, 117–119	202.37	mM	1	51.8	33.5	14.7	60.7	7.0	32.2	100.0	0.0	0.0	0.18	1.3
899A-9R-1, 32–34	158.62	M	1	44.2	16.8	38.9	72.4	7.5	20.1	99.0	0.0	0.9	0.27	1.0
900A-15R-2, 120–122	125.1	lM	1	52.6	29.2	18.2	64.3	4.9	30.8	100.0	0.0	0.0	0.14	0.7
900A-14R-1, 92–96	113.62	lM	1	62.4	24.1	13.5	72.2	7.4	20.4	100.0	0.0	0.0	0.27	6.7
900A-21R-3, 72–74	184.02	eM	1	66.8	26.1	7.1	71.9	7.0	21.1	100.0	0.0	0.0	0.25	0.3
900A-31R-1, 8–10	276.78	eM	1	35.5	61.4	3.0	36.6	14.7	48.7	100.0	0.0	0.0	0.23	1.3
			Avg	52.2	31.9	15.9	63.0	8.1	28.9	99.8	0.0	0.2	0.22	1.9
			Std	10.5	14.2	11.4	12.6	3.1	10.1	0.4	0.0	0.3	0.05	2.2
897C-48R-3, 51-52	507.41	eO	1	36.7	59.2	4.1	38.3	29.3	32.4	100.0	0.0	0.0	0.47	4.0
897C-44R-2, 85–87	467.65	lO	1	47.0	35.5	17.5	56.9	6.6	36.5	100.0	0.0	0.0	0.15	1.7
898A-33X-2, 4–6	304.34	lO	1	53.7	43.3	3.0	53.2	9.2	37.6	100.0	0.0	0.0	0.20	9.3
899B-7R-2, 14–16	284.64	lO	1	30.2	22.6	47.2	57.1	13.4	29.5	100.0	0.0	0.0	0.31	3.0
900A-38R-1, 91–93	345.11	lO	1	38.9	46.4	14.7	45.6	14.6	39.8	67.0	0.0	33.0	0.27	
			Avg	41.3	41.4	17.3	50.2	14.6	35.2	93.4	0.0	6.6	0.28	5.5
			Std	8.2	12.1	16.0	7.3	7.9	3.7	13.2	0.0	13.2	0.11	3.2
900A-66R-1, 114–116	615.24	mE	1	41.4	57.3	1.3	41.7	11.9	46.4	100.0	0.0	0.0	0.20	
900A-73R-2, 62–64	683.82	mE	1	41.8	53.7	4.5	43.0	13.9	43.0	73.0	9.0	18.0	0.24	
900A-74R-2, 6–8	692.96	mE	1	35.7	49.8	14.5	41.7	10.6	47.7	49.0	0.0	51.0	0.18	
900A-75R-2, 10–12	702.41	mE	1	53.4	43.7	3.0	54.5	5.4	40.1	88.0	13.0	0.0	0.12	8.0
			Avg	43.1	51.1	5.8	45.2	10.5	44.3	77.5	5.5	17.3	0.19	13.6
			Std	6.4	5.0	5.1	5.4	3.1	3.0	19.0	5.7	20.8	0.04	4.2
897A-1R-1, 19–21	0.19	P	2	65.3	33.1	1.6	66.4	9.1	24.5	100.0	0.0	0.0	0.27	4.7
897C-3R-1, 100–102	70.6	P	2	60.9	37.7	1.4	61.8	8.3	30.0	100.0	0.0	0.0	0.22	16.0
898A-14H-4, 106–108	128.82	P	2	60.2	34.1	5.7	63.8	15.1	21.1	100.0	0.0	0.0	0.42	13.3
898A-15X-3, 72–74	136.42	P	2	61.4	31.5	7.1	66.1	7.0	26.9	100.0	0.0	0.0	0.21	19.3
898A-12H-5, 30–32	110.52	P	2	68.8	25.0	6.3	73.3	8.1	18.5	100.0	0.0	0.0	0.31	30.0
898A-1H-4, 130–134	5.8	P	2	69.4	19.4	11.1	78.1	4.9	17.0	100.0	0.0	0.0	0.22	5.3
898A-4H-6, 109–111	36.79	P	2	71.9	24.1	4.0	74.9	6.5	18.6	100.0	0.0	0.0	0.26	14.0
898A-6H-4, 143–145	53.14	P	2	70.3	24.0	5.7	74.6	7.2	18.2	100.0	0.0	0.0	0.28	6.0
			Avg	66.0	28.6	5.4	69.9	8.3	21.9	100.0	0.0	0.0	0.27	13.6
			Std	4.4	5.9	2.9	5.7	2.8	4.4	0.0	0.0	0.0	0.06	8.0
897C-19R-1, 144–146	225.54	Pl	2	68.7	22.8	8.5	75.1	4.4	20.4	100.0	0.0	0.0	0.18	11.0
900A-37R-1, 24–26	334.74	eM	2	60.9	25.3	13.8	70.7	12.7	16.7	100.0	0.0	0.0	0.43	0.7
900A-42R-6, 48–50	390.88	lO	2	55.7	33.8	10.5	60.8	5.4	33.8	96.0	0.0	4.0	0.14	
897C-55R-1, 18–20	571.68	lE	2	39.6	34.7	25.8	53.3	11.4	35.3	100.0	0.0	0.0	0.24	2.3
897D-7R-1, 98–100	656.18	EC	2	58.8	7.9	33.3	87.6	8.2	4.1	21.0	3.0	75.0	0.67	4.0
			Avg	56.7	24.9	18.4	69.5	8.4	22.1	83.4	0.6	15.8	0.33	4.6
			Std	9.6	9.7	9.6	11.8	3.2	11.6	31.2	1.2	29.6	0.20	3.5
901A-1W-3, 21–28	2.43	J	2	15.9	1.7	82.4	90.4	9.6	0.0	34.0	0.0	66.0	1.00	0.7
901A-5R-1, 22–26	220.02	J	2	7.0	0.3	92.7	95.2	4.8	0.0	23.0	0.0	77.0	1.00	3.3
901A-6R-CC, 16–18	230.88	J	2	8.8	1.7	89.5	83.9	16.1	0.0	30.0	0.0	70.0	1.00	0.7
			Avg	10.6	1.2	88.2	89.8	10.2	0.0	29.0	0.0	71.0	1.00	1.6
			Std	3.8	0.7	4.3	4.6	4.6	0.0	4.5	0.0	4.5	0.00	1.2
897A-3R-1, 33–35	17.03	P	3	80.7	19.0	0.4	81.0	2.6	16.5	100.0	0.0	0.0	0.04	0.0
898A-11H-3, 88–90	98.6	P	3	78.9	20.6	0.4	79.3	1.8	18.9	100.0	0.0	0.0	0.09	4.3
897C-12R-1, 1–3	156.61	Pl	3	78.7	20.9	0.4	79.0	3.9	17.1	100.0	0.0	0.0	0.19	1.0
899A-3R-3, 18–20	103.98	Pl	3	63.2	18.4	18.4	77.5	4.5	18.0	100.0	0.0	0.0	0.20	1.0
			Avg	75.4	19.7	4.9	79.2	3.2	17.6	100.0	0.0	0.0	0.13	1.6
			Std	7.1	1.1	7.8	1.2	1.1	0.9	0.0	0.0	0.0	0.07	1.6
897C-64R-1, 7–9	658.47	EC	4	53.8	34.3	11.9	61.1	3.4	35.6	3.6	0.0	96.0	0.09	1.2

Notes: See Table 1 for definition of recalculated parameters. Grain size: 4 = coarse sand; 3 = medium sand; 2 = fine sand; 1 = very fine sand. Age: P = Pleistocene; Pl = Pliocene (late [1P1]); M = Miocene (early [eM], middle [mM] and late [1M]); O = Oligocene (early [eO] and late [1O]); E = Eocene (middle [mE] and late [IE]); EC = Early Cretaceous; J = Jurassic.

Sand Provenance

The Leg 149 sites are located in an embayment of the Iberia Abyssal Plain, between the Galicia Bank and the Estremadura Spur (Fig. 1). General bathymetry around the sites suggests that terrigenous components within the cored successions were most likely derived from the Iberia Margin, or perhaps the Galicia Bank. Bathymetry of the Iberian continental slope to the east of the Leg 149 transect shows a series of submarine canyons and valleys that potentially funnel(ed) sandy sediment out to the Iberia Abyssal Plain, at least back through the Pliocene, and perhaps throughout the Tertiary.

For the most part, the monomineralic and lithic components of the Leg 149 sand and sandstone are consistent with derivation from felsic plutonic and metamorphic terrains, similar to the Hercynian basement rocks (Variscan Belt) of the northwestern Iberian Peninsula (Galicia-Tras-Os-Montes Zone; Azor et al., 1994; Capdevila and

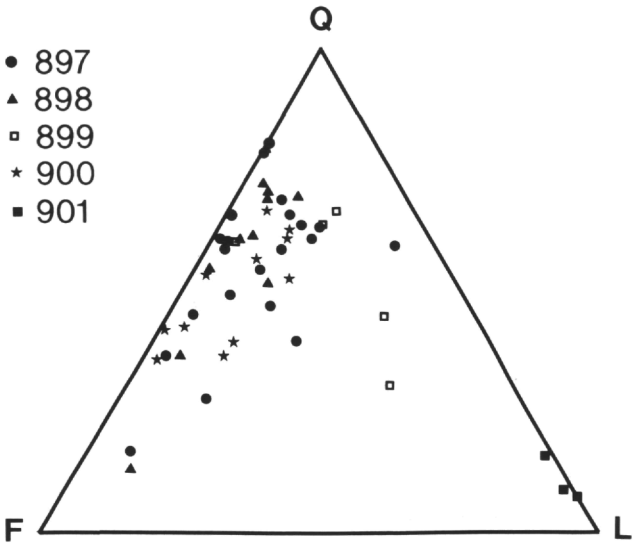

Figure 5. QFL ternary plot of Leg 149 petrographic data by site.

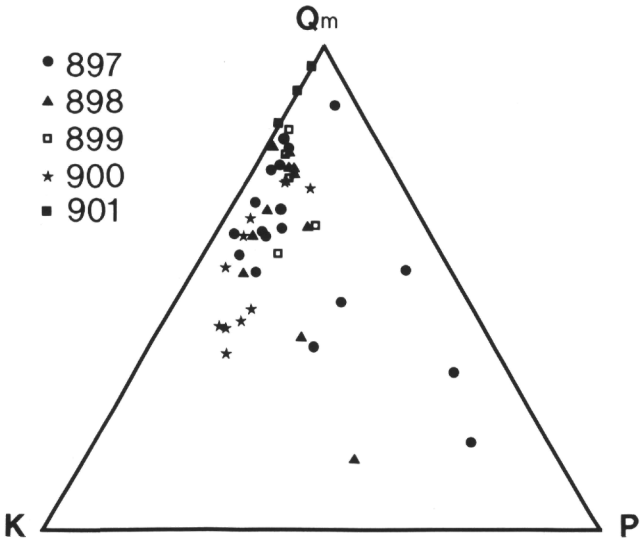

Figure 6. QmKP ternary plot of Leg 149 petrographic data by site. Minor etched, but unstained, feldspar (albite) was counted separately (Fu category; Appendix), but ultimately grouped with plagioclase in calculating P for this plot.

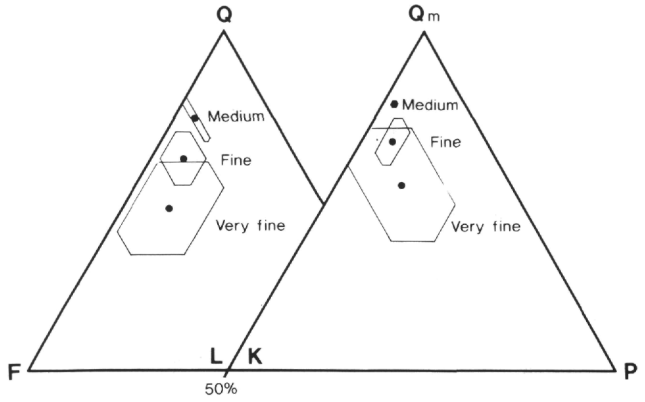

Figure 7. QFL (left) and QmKP (right) ternary plots of detrital modes for medium, fine, and very fine sand subsets for all Cenozoic samples. Polygons represent the fields of variation (standard deviations) about mean values.

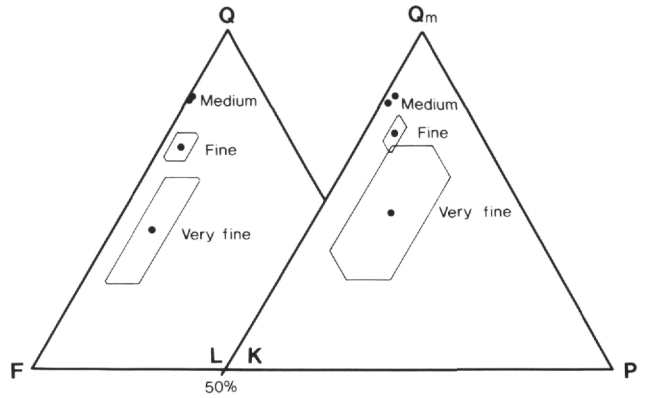

Figure 8. QFL (left) and QmKP (right) ternary plots of detrital modes for medium, fine, and very fine sand subsets for Pleistocene samples. Polygons represent the fields of variation (standard deviations) about mean values.

Mougenot, 1988). Precambrian to Paleozoic felsic plutonic and metamorphic rocks crop out over much of the drainage basins of the major rivers (i.e., Rio Duero, Rio Minho, and Rio Mondego) that presently empty onto the Iberian shelf north of latitude 40°N (Fig. 12). As discussed below, similar basement rocks also comprise the Galicia Bank, and so in terms of composition both the Galicia Bank and Iberian mainland (massif) are plausible sources of sand. However, there is no evidence to suggest that the Galicia Bank was emergent during the early Cenozoic (Winterer et al., 1988), and therefore it was not likely a major source of Cenozoic sand at Leg 149 sites. Thus, the Iberian mainland most likely supplied the terrigenous component within the Cenozoic sequences cored on Leg 149.

However, the Mesozoic picture of sand provenance is less clear. The shelf and onshore regions to the east-southeast of the Leg 149 transect were dissected into a series of horsts and grabens during rift-related extension in the late Triassic/Early Jurassic, forming, in part, the Lusitanian Basin (Wilson and Exton, 1979; Montenat et al., 1988); faults within this region were rejuvenated during the Late Jurassic and Early Cretaceous (Wilson and Exton, 1979; Montenat et al., 1988). This extension and dissection may have served to trap mainland-derived sand, limiting its offshore distribution. During this same time frame, sand was shed to the west off the emergent basement highlands of the Galicia Bank and deposited by turbidity currents at Leg 103 sites (Fig. 1; Winterer et al., 1988; Johnson, 1988). This sand is quartzofeldspathic with a minor lithic component, and its composition suggests a basement source composed of felsic plutonic and metamorphic rocks (Winterer et al., 1988; Johnson, 1988) which is not only similar to dredged samples from the Galicia Bank (Capdevila and Mougenot, 1988), but also to the rocks of the Iberian mainland (Winterer et al., 1988).

Sandstone detrital modes calculated by Johnson (1988) for 31 very fine sandstones of Cretaceous age from Leg 103 are similar to those of Cenozoic samples from Leg 149; Johnson's data cluster about a mean value of 52:36:12 %QFL, which is almost the same as the Leg 149 Pliocene mean in Figure 9 (52:38:10 %QFL). In general, Mesozoic samples from the Leg 149 sites (Fig. 11) contain significantly less feldspar than the Leg 103 Mesozoic samples. This difference is not a function of variation in techniques between the two studies, in that Johnson (1988) employed petrographic and staining methods identical to those of our study. The similarity of the Leg 103 Cretaceous samples and Leg 149 Pliocene samples could be a function of grain size, as discussed previously, or may be related to the

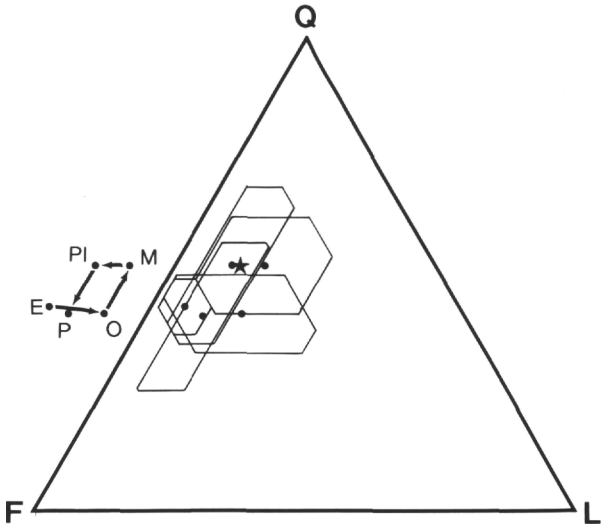

Figure 9. QFL ternary plot of Cenozoic very fine sand detrital modes (see Table 2 for values). Polygons represent the fields of variation (standard deviations) about mean values (solid circles) for various epochs. The pattern of distribution of means has been reproduced to the left of the ternary plot to better outline compositional shifts through time (arrows). E = Eocene; O = Oligocene; M = Miocene; Pl = Pliocene; P = Pleistocene. Star = mean value for Leg 103 Cretaceous sandstones from Johnson (1988).

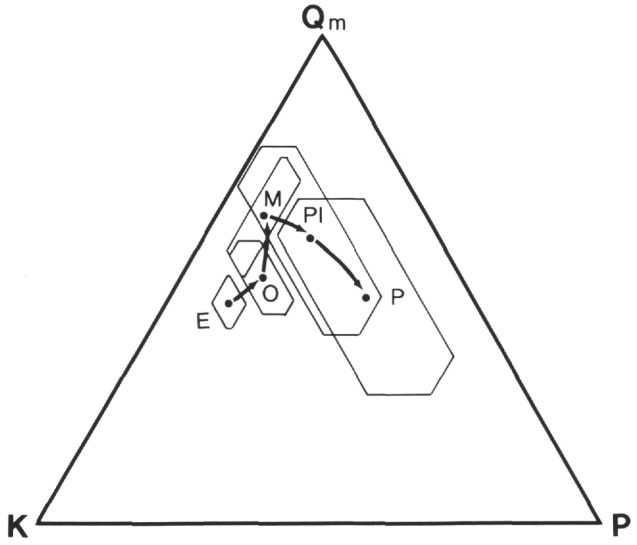

Figure 10. QmKP ternary plot of Cenozoic very fine sand detrital modes (see Table 2 for values). Polygons represent the fields of variation (standard deviations) about mean values for various epochs. Arrows connect progressively younger means and outline temporal shifts in composition. Abbreviations as in Figure 9.

similarity of sand source regions. Perhaps the ratio of metamorphic/plutonic exposures on the Galicia Banks "paleoland" was similar to that of northwestern Iberia during the Pliocene. Of course, other provenance factors such as climate and associated weathering intensity may have also played a role. Although Cretaceous sands derived from the Galicia Bank are dissimilar to the few Leg 149 Cretaceous sandstones analyzed for this study, given the likely spatial variations in basement lithology across the Galicia Bank, a northern source for the Leg 149 Mesozoic sand cannot be ruled out.

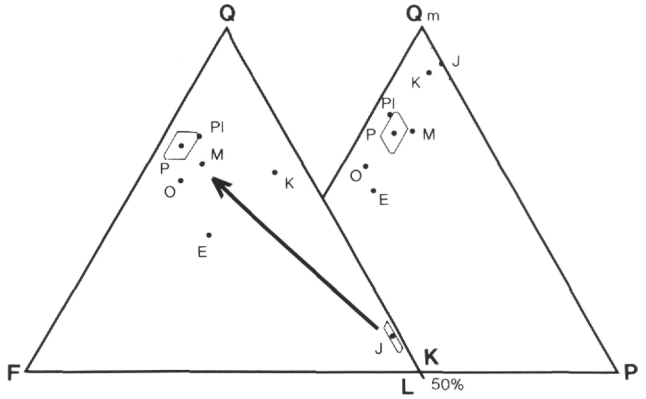

Figure 11. QFL (left) and QmKP (right) ternary plots of fine sand detrital modes. Means and fields of variation (polygons) are plotted for time intervals represented by multiple samples (Jurassic [J], *n* - 3; Pleistocene [P], *n* = 8), and individual samples are plotted for the remaining time intervals (K = Cretaceous; abbreviations as in Fig. 9). The arrow defines the general temporal trend.

Temporal Changes in Composition and Passive Margin Evolution

A number of studies of modern and ancient sand have examined passive margin provenance, and of these, most focus on ancient sequences and emphasize the high quartz content of these sediments (e.g., Schwab, 1975; Dickinson and Valloni, 1980; Ingersoll and Suczek, 1979). Only one study (i.e., Marsaglia, 1991) explores the relationship of sand provenance to the rift-to-drift evolution of passive margins. The Leg 149 data presented in Table 2 are therefore noteworthy because they represent a semicontinuous Cenozoic to Mesozoic sedimentary sequence that accumulated during a rift-to-drift transition along the Iberian passive margin.

The series of temporal trends outlined in Figures 9 through 11 and discussed above cannot be rigorously modeled, but can be linked to the tectonic evolution of this margin. The QFL trend depicted by the arrow in Figure 11 is a crude evolutionary path that more accurately consists of a major jump from Jurassic lithoclastic sand to more quartzofeldspathic post-Jurassic sand. Similar evolutionary pathways have been proposed for sand detrital modes from other tectonic settings, some of which are thought to represent unroofing trends (e.g., Dickinson, 1985; Marsaglia et al., 1992). Progressive variation within the lithic populations of the Leg 149 fine sand also suggests an unroofing trend for this margin. Mesozoic sandstones are sedimenticlastic, whereas the Cenozoic sandstones largely contain metamorphic clasts and exhibit progressively smaller lithic proportions, to the point where they are quartzofeldspathic (see data in Table 2). This pattern could grossly reflect the progressive removal of first sedimentary, and then metamorphic, cover of plutonic basement rocks. In terms of the provenance fields of Dickinson and Suczek (1979), this trend would correspond to passing from recycled orogen provenance (synrift to postrift phases?) to continental block provenance (postrift to drift phases?). Obviously, more data are needed to clarify the nature of this trend and to determine if such a trend is specific to this segment of the Iberia Margin or is more representative of passive margin sequences as a whole.

Compositional trends within the very fine sand samples may represent a regional tectonic overprint unrelated to the passive margin setting. This tectonic overprint is a Tertiary compressional phase that caused inversion of basin structures and probably uplifted onshore source terrains. The shift to more lithic-rich (Fig. 9) and quartzose (Fig. 10) sand compositions in the Oligocene and Miocene could therefore be linked to uplift of metamorphic terrains and/or drainage rearrangement, and the subsequent shift toward more quartzofelds-

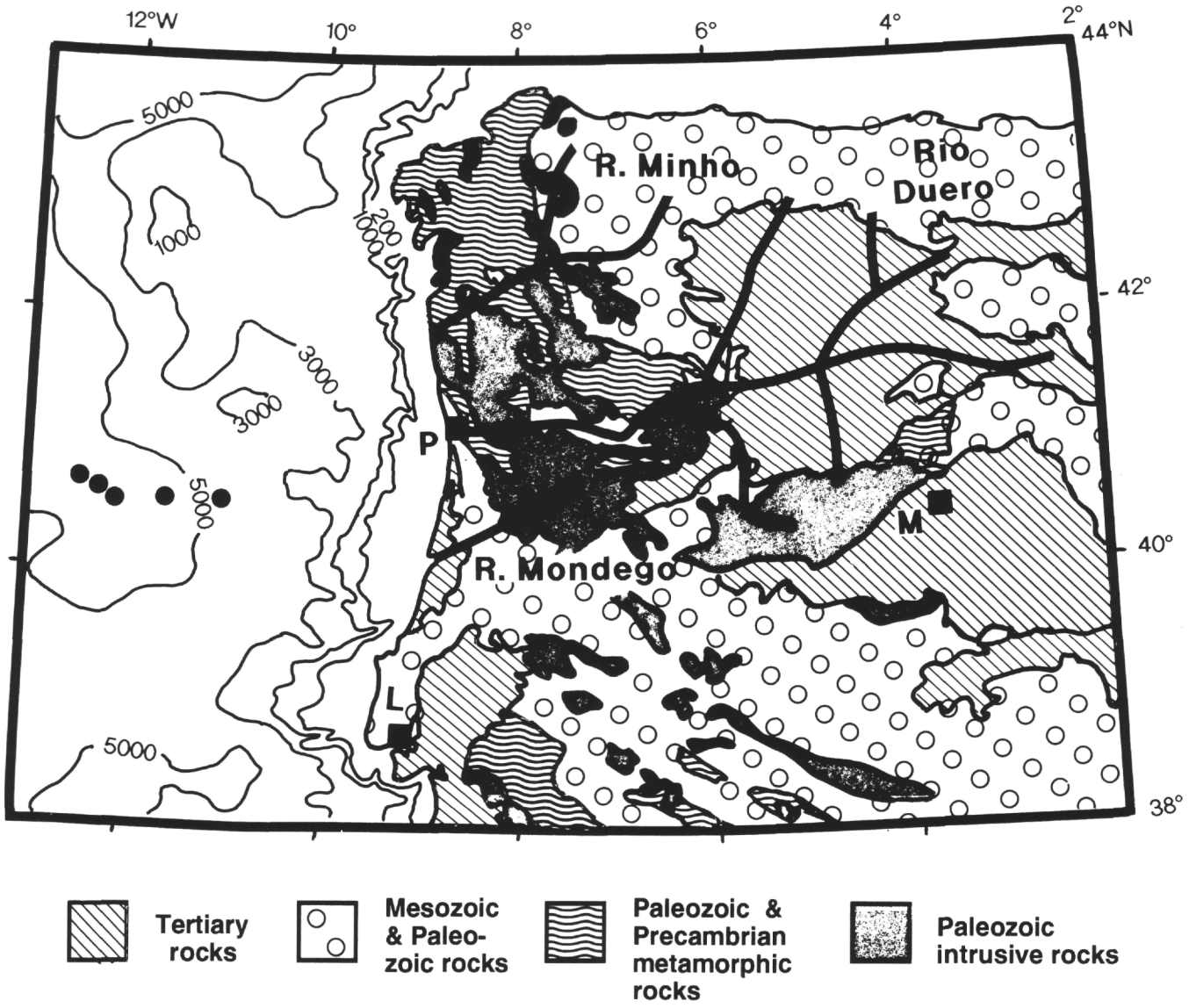

Figure 12. Simplified geologic map of the northwestern Iberian Peninsula, with locations of major river (rio) drainages discussed in text. Solid circles mark approximate locations of Leg 149 sites. Bathymetry is in meters. Modified from Choubert (1971).

pathic sand compositions in the Pliocene and Pleistocene could be linked to the removal of metamorphic cover and exposure of underlying plutonic sequences.

The small (n = 50) data set presented here suggests that models for passive margin sequences based on sand detrital modes are plausible and that passive margin sequences are perhaps more complex than previously thought. Of course, in our brief discussion we simplify the story in that we emphasize the large-scale tectonic controls on the Leg 149 sand detrital modes and downplay other provenance factors. For example, we do not address the possible effects of the major climatic changes that also occurred during the evolution of this margin. More subtle variations in feldspar composition could be linked to these climatic changes, particularly with respect to the intensity of weathering, but given the small sample number, we thought this somewhat imprudent.

CONCLUSIONS

Sand recovered on ODP Leg 149 is predominantly quartzofeldspathic with a lesser metamorphic and sedimentary lithic component. There appears to be a distinct link between grain size and composition within the Cenozoic samples, probably because of a combination of transport and depositional history. Fine sand detrital modes reflect the overall passive margin, rift-to-drift evolution and show a crude basement unroofing trend from the Mesozoic to the Cenozoic. The detrital modes of Cenozoic very fine sand are a function, to some degree, of a superposed compressional tectonic event that resulted in a minor increase in metamorphic lithic content during the Oligocene and Miocene, perhaps associated with enhanced uplift(?) on the adjacent Iberia Peninsula.

ACKNOWLEDGMENTS

This project was supported by a grant to Marsaglia from the National Science Foundation and Joint Oceanographic Institutions administered by the Texas A&M Research Foundation. The Research Careers for Minority Students Program at UT El Paso (funded by the National Science Foundation) provided additional support for Padilla. We thank Andrew Morton, Douglas Masson, and an anonymous reviewer for their helpful comments.

REFERENCES

Azor, A., Lodeiro, F.G., and Simancas, J.F., 1994. Tectonic evolution of the boundary between the Central Iberian and Ossa-Morena zones (Variscan belt, southwest Spain). *Tectonics,* 13:45-61.

Capdevila, R., and Mougenot, D., 1988. Pre-Mesozoic basement of the western Iberian continental margin and its place in the Variscan Belt. *In* Boillot, G., Winterer, E.L., et al., *Proc. ODP, Sci. Results,* 103: College Station, TX (Ocean Drilling Program), 3-12.

Choubert, G., 1971. International geological map of Europe and the Mediterranean region, western sheet. Bundesanst. Bodenforsch./UNESCO, Hannover, Germany (scale 1:5,000,000).

Dickinson, W.R., 1970. Interpreting detrital modes of graywacke and arkose. *J. Sediment. Petrol.,* 40:695-707.

————, 1985. Interpreting provenance relations from detrital modes of sandstones. *In* Zuffa, G.G. (Ed.), *Provenance of Arenites:* Dordrecht (D. Riedel), 333-361.

Dickinson, W.R., and Suczek, C.A., 1979. Plate tectonics and sandstone compositions. *AAPG Bull,* 63:2164-2182.

Dickinson, W.R., and Valloni, R., 1980. Plate settings and provenance of sands in modern ocean basins. *Geology,* 8:82-86.

Ingersoll, R.V., Bullard, T.F., Ford, R.L., Grimm, J.P., Pickle, J.D., and Sares, S.W., 1984. The effect of grain size on detrital modes: a test of the Gazzi-Dickinson point-counting method. *J. Sediment. Petrol.,* 54:103-116.

Ingersoll, R.V., and Suczek, C.A., 1979. Petrology and provenance of Neogene sand from Nicobar and Bengal Fans, DSDP Sites 211 and 218. *J. Sediment. Petrol.,* 49:1217-1228.

Johnson, J.A., 1988. Composition of Lower Cretaceous sandstone, Galicia Margin. *In* Boillot, G., Winterer, E.L., et al., *Proc. ODP, Sci. Results,* 103: College Station, TX (Ocean Drilling Program), 505-512.

Kairo, S., Suttner, L.J., and Dutta, P.K., 1993. Variability in sandstone composition as a function of depositional environment in coarse-grained delta system. *In* Johnsson, M.J., and Basu, A. (Eds.), *Processes Controlling the Composition of Clastic Sediments:* Spec. Pap.—Geol. Soc. Am., 284:41-65

Marsaglia, K.M., 1991. Provenance of sands and sandstones from a rifted continental arc, Gulf of California, Mexico. *In* Fisher, R.V., and Smith, G.A. (Eds.), *Sedimentation in Volcanic Settings.* Spec. Publ.—Soc. Econ. Paleontol. Mineral., 45:237-248.

Marsaglia, K.M., Ingersoll, R.V., and Packer, B.M., 1992. Tectonic evolution of the Japanese Islands as reflected in modal compositions of Cenozoic forearc and backarc sand and sandstone. *Tectonics,* 11:1028-1044.

Marsaglia, K.M., and Tazaki, K., 1992. Diagenetic trends in Leg 126 sandstones. *In* Taylor, B., Fujioka, K., et al., *Proc. ODP, Sci. Results,* 126: College Station, TX (Ocean Drilling Program), 125-138.

Montenat, C., Guery, F., Jamet, M., and Berthou, Y.B., 1988. Mesozoic evolution of the Lusitanian Basin: comparison with the adjacent margin. *In* Boillot, G., Winterer, E.L., et al., *Proc. ODP, Sci. Results,* 103: College Station, TX (Ocean Drilling Program), 757-775.

Sawyer, D.S., Whitmarsh, R.B., Klaus, A., et al., 1994. *Proc. ODP, Init. Repts.,* 149: College Station, TX (Ocean Drilling Program).

Schwab, F.L., 1975. Framework mineralogy and chemical composition of continental margin-type sandstone. *Geology,* 3:487-490.

Sedimentation Seminar, 1988. Comparative petrographic maturity of river and beach sand, and origin of quartz arenites. *J. Geol. Educ.,* 36:79-87.

Whitmarsh, B., Sawyer, D.S., and ODP Leg 149 Scientific Party, 1994. Upper mantle drilling in the ocean-continent transition west of Iberia. *Terra Nova,* 5:327-331.

Wilson, R.C., and Exton, J., 1979. Mesozoic development of the Lusitanian Basin, West-Central Portugal. *In* Wilson, R.C., and Exton, J. (Eds.), *Excursion to the Mesozoic of the Lusitanian Basins, West-Central Portugal* (Pt. II). Dept. Earth Sci., Open Univ., 45-77.

Winterer, E.L., Gee, J.S., and Van Waasbergen, R.J., 1988. The source area for Lower Cretaceous clastic sediments of the Galicia Margin: geology and tectonic and erosional history. *In* Boillot, G., Winterer, E.L., et al., *Proc. ODP, Sci. Results,* 103: College Station, TX (Ocean Drilling Program), 697-732.

Date of initial receipt: 5 December 1994
Date of acceptance: 20 July 1995
Ms **149SR-201**

APPENDIX. PETROGRAPHIC DATA

Core, section, interval (cm)	Depth (mbsf)	Qp	Qm	P	K	Fu	Lv	Lmm	Lmt	Lma	Lsa	Lsch	Lsc	Mus	Biot	Op	D	Bio	Glau	Other	Pl	Carb	Serp	Points
149-897A-																								
1R-1, 19–21	0.19	1	159	19	59	3	0	2	2	0	0	0	0	5	9	1	1	36	3	0	0	0	0	300
3R-1, 33–35	17.03	2	219	7	45	0	0	0	1	0	0	0	0	0	0	3	1	20	2	0	0	0	0	300
6R-5, 11–13	51.71	0	124	11	32	0	0	15	22	0	0	0	0	5	40	0	0	37	0	5	9	0	0	300
149-897C-																								
2R-1, 142–144	61.32	0	22	80	17	0	0	2	7	0	0	1	0	9	89	6	0	65	0	0	2	0	0	300
3R-1, 100–102	70.6	2	132	18	65	0	0	2	1	0	0	0	0	3	45	5	0	24	1	0	2	0	0	300
7R-1, 86–88	109.06	1	53	38	8	0	0	2	6	0	0	0	2	6	59	35	1	31	2	0	56	0	0	300
8R-1, 92–94	118.82	0	38	65	11	0	0	10	11	0	0	0	0	12	86	43	0	21	0	0	3	0	0	300
10R-2, 8–10	138.78	0	125	7	52	0	0	6	20	4	0	0	0	2	14	0	2	67	1	0	0	0	0	300
12R-1, 1–3	156.61	4	218	11	48	0	0	0	1	0	0	0	0	1	2	0	0	13	0	2	0	0	0	300
14R-3, 104–106	179.84	0	86	16	36	0	0	1	4	0	0	0	0	8	83	19	3	39	2	0	3	0	0	300
19R-1, 144–146	225.54	0	169	10	46	0	0	0	19	2	0	0	0	2	31	0	0	21	0	0	0	0	0	300
22R-3, 9–11	256.09	0	152	12	40	0	0	0	26	1	0	0	0	3	17	21	1	21	0	0	6	0	0	300
23R-2, 109–111	265.29	0	69	43	34	0	0	3	4	0	0	0	0	4	65	0	1	15	0	0	62	0	0	300
24R-1, 78–80	273.08	5	140	6	44	0	0	5	29	0	0	0	0	12	19	3	3	33	1	0	0	0	0	300
25R-CC, 0–2	283.98	0	119	19	58	0	0	2	4	1	0	0	0	6	58	9	0	12	1	0	11	0	0	300
44R-2, 85–87	467.65	0	78	9	50	0	0	2	27	0	0	0	0	1	4	0	2	124	3	0	0	0	0	300
48R-3, 51–52	507.41	0	72	55	61	0	0	0	8	0	0	0	0	1	11	1	0	91	0	0	0	0	0	300
55R-1, 18–20	571.68	0	89	18	59	1	0	7	51	0	0	0	0	0	7	0	0	66	2	0	0	0	0	300
64R-1, 7–9	658.47	0	127	2	74	5	0	0	1	0	3	0	24	0	3	0	0	11	0	0	0	0	0	250
149-897D-																								
7R-1, 98–100	656.18	8	149	7	7	7	3	5	13	1	50	0	17	0	12	5	2	0	0	14	0	0	0	300
149-898A-																								
1H-4, 130–134	5.8	9	166	11	38	0	0	9	19	0	0	0	0	2	14	0	0	32	0	0	0	0	0	300
4H-6, 109–111	36.79	1	160	14	40	0	0	0	9	0	0	0	0	4	38	0	2	32	0	0	0	0	0	300
5H-4, 49–51	42.72	2	71	49	63	0	0	7	5	0	0	0	1	1	54	4	0	36	5	0	2	0	0	300
6H-4, 143–145	53.14	0	135	13	33	0	0	2	8	1	0	0	0	2	16	0	0	90	0	0	0	0	0	300
11H-3, 88–90	98.6	6	174	4	43	0	0	1	0	0	0	0	0	7	6	0	0	58	0	1	0	0	0	300
12H-5, 30–32	110.52	1	98	11	25	0	0	3	6	0	0	0	0	14	76	2	0	64	0	0	0	0	0	300
14H-4, 106–108	128.82	6	121	30	42	0	0	4	8	0	0	0	0	6	34	13	0	31	0	0	5	0	0	300
15X-3, 72–74	136.42	1	112	12	46	0	0	1	12	0	0	0	0	8	50	10	0	45	2	0	1	0	0	300
18X-1, 142–145	159.52	0	9	29	22	0	0	3	2	0	0	0	1	5	102	8	0	86	2	0	31	0	0	300
22X-4, 117–119	202.37	0	130	13	69	2	0	4	33	0	0	0	0	0	4	0	1	37	7	0	0	0	0	300
33X-2, 4–6	304.34	12	133	23	94	0	0	0	8	0	0	0	0	11	17	1	1	nc	0	0	0	0	0	300
149-899A-																								
3R-3, 18–20	103.98	5	167	10	40	0	0	15	35	0	0	0	0	0	3	0	0	18	2	0	0	5	0	300
5R-1, 33–35	120.43	9	171	5	33	0	0	2	51	0	0	0	0	5	18	0	1	4	1	0	0	0	0	300
6R-1, 37–39	130.07	0	160	43	50	0	0	3	10	0	0	0	0	2	9	3	0	13	6	0	1	0	0	300
9R-1, 32–34	158.62	2	124	13	35	0	0	32	73	5	1	0	0	1	2	0	3	7	1	0	0	0	1	300
149-899B-																								
7R-2, 14–16	284.64	0	64	15	33	0	0	13	87	0	0	0	0	5	4	0	0	78	1	0	0	0	0	300
149-900A-																								
14R-1, 92–96	113.62	1	165	17	47	0	0	5	30	1	0	0	0	0	20	1	1	0	12	0	0	0	0	300
15R-2, 120–122	125.1	5	139	11	69	0	0	7	43	0	0	0	0	0	2	0	3	3	17	1	0	0	0	300
21R-3. 72–74	184.02	0	123	12	36	0	0	3	10	0	0	0	0	1	0	0	0	112	3	0	0	0	0	300
31R-1, 8–10	276.78	1	69	28	93	0	0	4	2	0	0	0	0	1	3	2	0	94	3	0	0	0		300
37R-1, 24–26	334.74	8	98	19	25	0	0	7	17	0	0	0	0	2	0	0	0	124	0	0	0	0	0	300
38R-1, 91–93	345.11	0	103	21	90	12	0	2	23	1	13	0	0	3	25	3	1	nc	3	0	0	0	0	300
42R-6, 48–50	390.88	8	124	5	69	6	0	6	17	1	1	0	0	3	10	0	0	nc	0	0	0	0	0	250
66R-1, 114–116	615.24	1	98	24	109	4	0	0	3	0	0	0	0	21	37	0	1	nc	2	0	0	0	0	300
73R-2, 62–64	683.82	3	99	21	99	11	1	0	6	2	2	0	0	17	29	2	4	nc	4	0	0	0	0	300
74R-2, 6–8	692.96	0	91	21	104	2	0	4	14	0	13	0	6	12	23	2	1	nc	0	7	0	0	0	300
75R-2, 10–12	702.41	3	140	9	103	5	1	0	7	0	0	0	0	11	13	4	4	0	0	0	0	0	0	300
149-901A-																								
1W-3, 21–28	2.43	0	47	1	0	4	0	8	74	0	101	0	60	0	2	3	0	0	0	0	0	0	0	300
5R-1, 22–26	220.02	0	20	0	0	1	1	9	51	1	102	0	102	0	10	3	0	0	0	0	0	0	0	300
6R-CC, 16–18	230.88	0	26	0	0	5	0	11	67	1	132	0	53	0	2	2	1	0	0	0	0	0	0	300

Note: Counted categories are defined in Table 1; nc = not counted.

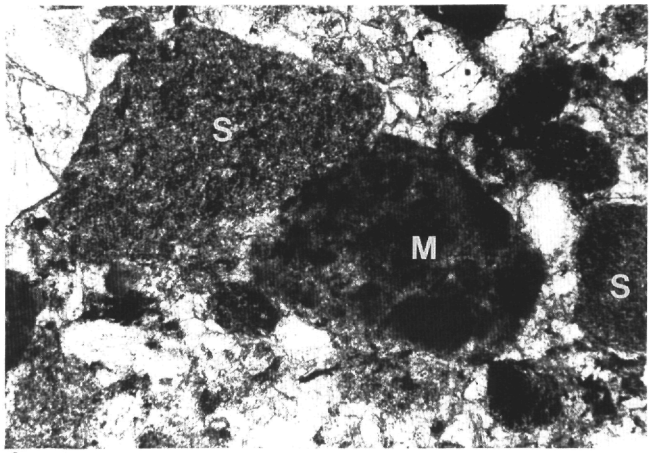

1

2

3

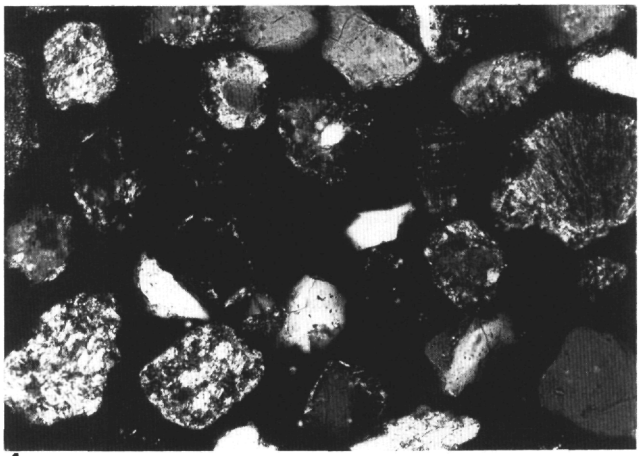

4

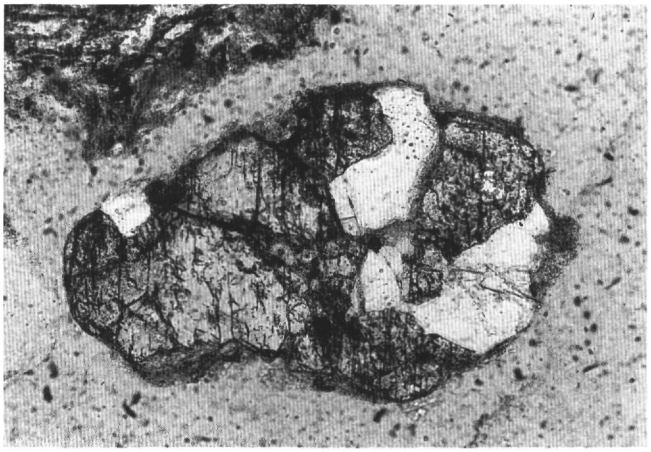

5

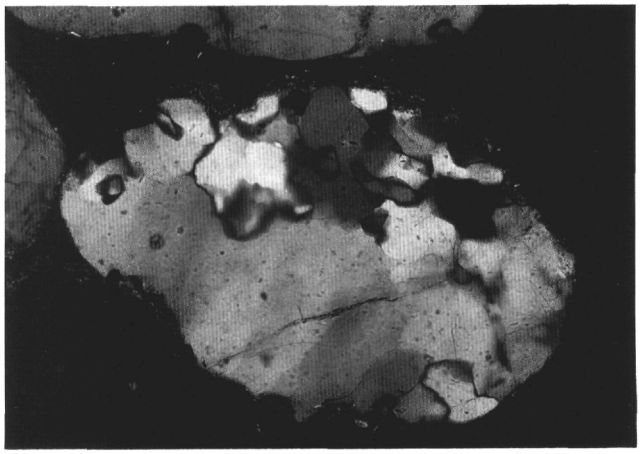

6

Plate 1. **1.** Sedimentary lithic fragments (S) and micritic carbonate lithic fragment (M) in Sample 149-901 A-1W-3, 28-31 cm. Scale bar = 0.2 mm. Plane-polarized light. **2.** Subparallel-arranged biotite and muscovite flakes in Sample 149-900A-74R-2, 6-8 cm. Scale bar = 0.2 mm. Plane-polarized light. **3.** Quartz-mica tectonite fragments (L) and grains of garnet (G) and glauconite (P) in Sample 149-899A-9R-1, 32-34 cm. Scale bar = 0.1 mm. Plane-polarized light. **4.** Same view as in Figure 3 with crossed nicols. **5.** Plutonic (quartz and potassium feldspar) rock fragment in Sample 149-898A-11H-3, 88—90 cm. Feldspar appears gray because it is etched and stained. Scale bar = 0.1 mm. Plane-polarized light. **6.** Rounded polycrystalline quartz fragment in Sample 149-898A-11H-3, 88-90 cm. Scale bar = 0.1 mm. Crossed nicols.

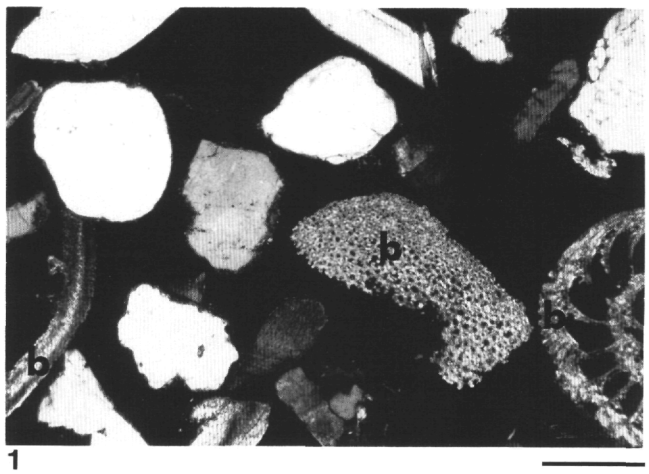

1

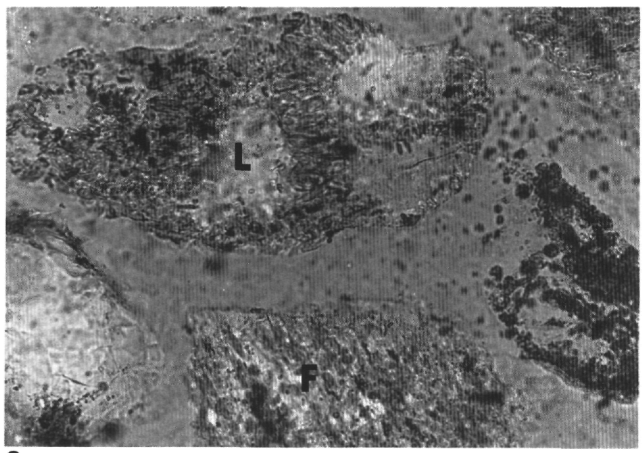

2

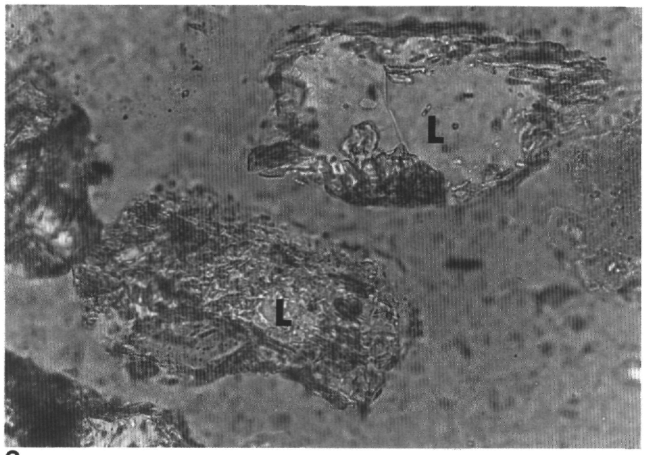

3

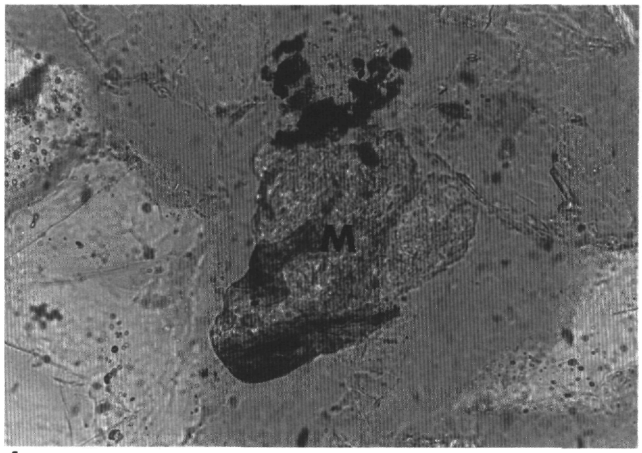

4

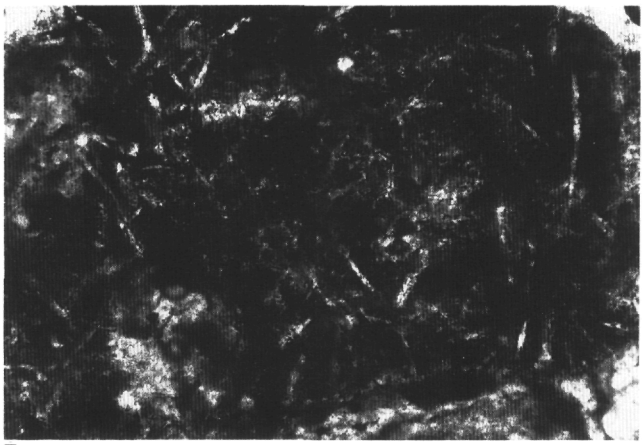

5

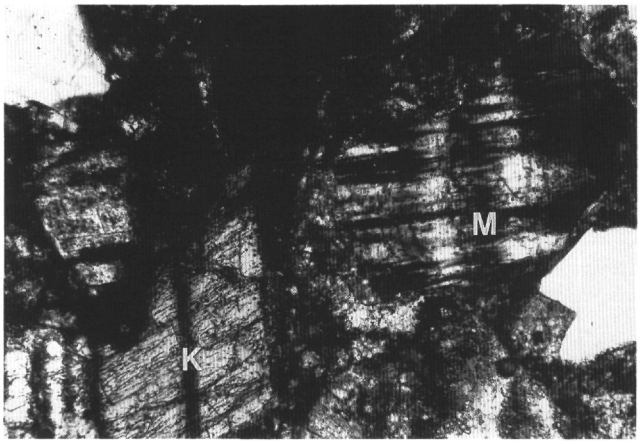

6

Plate 2. **1.** Rounded to subangular monocrystalline quartz (white) and biogenic clasts (b) in Sample 149-898A-11H-3, 88-90 cm. Bioclasts include foraminifer, pelecypod, and echinoderm fragments. Scale bar = 0.4 mm. Crossed nicols. **2.** Fine-grained, quartz-mica tectonite fragment (L) and partially altered plagioclase feldspar (F) in Sample 149-898A-1H-4, 130-134 cm. Scale bar = 0.05 mm. Plane-polarized light. **3.** Quartz-mica tectonite lithic fragments (L) in Sample 149-898A-1H-4, 130-134 cm. Scale bar = 0.05 mm. Plane-polarized light. **4.** Polycrystalline mica (M) in Sample 149-898A-1H-4, 130-134 cm. Scale bar = 0.05 mm. Crossed nicols. **5.** Volcanic lithic fragment in Sample 149-897C-62R-3, 77-79 cm. Scale bar = 0.2 mm. Plane-polarized light. **6.** Microcline (M) with tartan twinning and other potassium feldspar (K) in Sample 149-897C-64R-1, 34-36 cm. Scale bar = 0.2 mm. Crossed nicols.